IEEE Access
Multidisciplinary ⋮ Rapid Review ⋮ Open Access Journal

Received 23 December 2023, accepted 12 January 2024, date of publication 19 January 2024, date of current version 31 January 2024.

Digital Object Identifier 10.1109/ACCESS.2024.3355953

RESEARCH ARTICLE

Wideband Millimetre-Wave Dielectric Resonator Antenna Fed by a Wide Aperture

KING TUNG LO, (Student Member, IEEE), AND HANG WONG, (Fellow, IEEE)
State Key Laboratory of Terahertz and Millimeter Waves, Department of Electrical Engineering, City University of Hong Kong, Hong Kong

Corresponding author: Hang Wong (hang.wong@cityu.edu.hk)

This work was supported in part by the National Natural Science Foundation of China under Grant 62071408; and in part by the Research Grants Council of the Hong Kong, SAR, China, under Project CityU 11215522.

ABSTRACT This work presents a millimetre-wave (mmW) dielectric resonator antenna (DRA) excited by a wide aperture for bandwidth enhancement on the DRA and its array. The proposed antenna consists of a rectangular DRA top loaded with a metallic patch to produce two DRA modes on the radiator. The wide aperture is etched on the top metallic surface of a substrate-integrated waveguide (SIW) for contributing a slot mode and exciting the DRA. The proposed aperture is relatively wider than the conventional means of aperture-coupled DRAs, its size is almost identical to the base area of the DRA. An intensive parametric study proved using a wide aperture for excitation can lower the reactance of the higher-order mode of the DRA and thus expand the bandwidth. In addition, a 16-element DRA array with a 1-to-8 full corporate feeding network is introduced. A prototype of the array was fabricated and measured. The array exhibits a wide impedance bandwidth of 35.5% from 25.5 to 36.5 GHz for the reflection coefficient $\leq$ -10 dB and the maximum gain of 18.5 dBi. Throughout the operating bandwidth, stable broadside radiation patterns can be observed. A good agreement between the measured and simulated results can be obtained, which confirms these proposed designs found potential applications in the mmW wireless communication systems.

INDEX TERMS Dielectric resonator (DR) antenna (DRA), millimetre-wave (mmW) antenna, wide bandwidth.

I. INTRODUCTION

Millimetre-wave (mmW) technology attracts great attention due to its high data rate and huge available spectrum, favouring the development of wideband antenna designs [1]. Antennas and arrays with high-gain characteristics are desired in the mmW applications to compensate for significant propagation losses during wireless signals in transmission and reception [2].

Dielectric resonator antenna (DRA) was first introduced by Long et al. in 1983 [3]. It has been extensively investigated because of its compact structure, high gain, and high radiation efficiency due to the absence of conductive losses [4]. Conventional DRAs operate at the fundamental mode [5], [6] of the radiating dielectric body which produces a narrow bandwidth. Previous studies showed that the bandwidth of DRA can be enhanced in microwave bands through embedded structures [7], [8], and special shapes of DRA [9], [10], [11], [12]. However, it is challenging to apply these schemes to the mmW frequencies because they require high precision in antenna fabrications. Thus far, substrate-integrated DRA (SIDRA) [13], [14] and connected DRA [15], [16] have been developed to achieve wideband characteristics in the mmW band without difficulties in dealing with small and complicated structures. Unfortunately, most of the aforementioned DRA has a relatively large projection area, which requires a large element spacing in array implementation and thus limits the array radiation performance such as larger sidelobe levels and lower directivity. Meanwhile, the connected DRA [15], [16] uses the microstrip line feeding mechanism, which leads to a large back lode radiation in the mmW band.

Recently, researchers have demonstrated many outstanding DRA arrays [17], [18], [19], [20], [21], [22], [23], [24], [25] to have good radiation characteristics at the mmW frequency. However, most of the reported designs [17], [18], [19], [20], [21], [22], [23] exhibited good performance within

The associate editor coordinating the review of this manuscript and approving it for publication was Zaharias D. Zaharis.

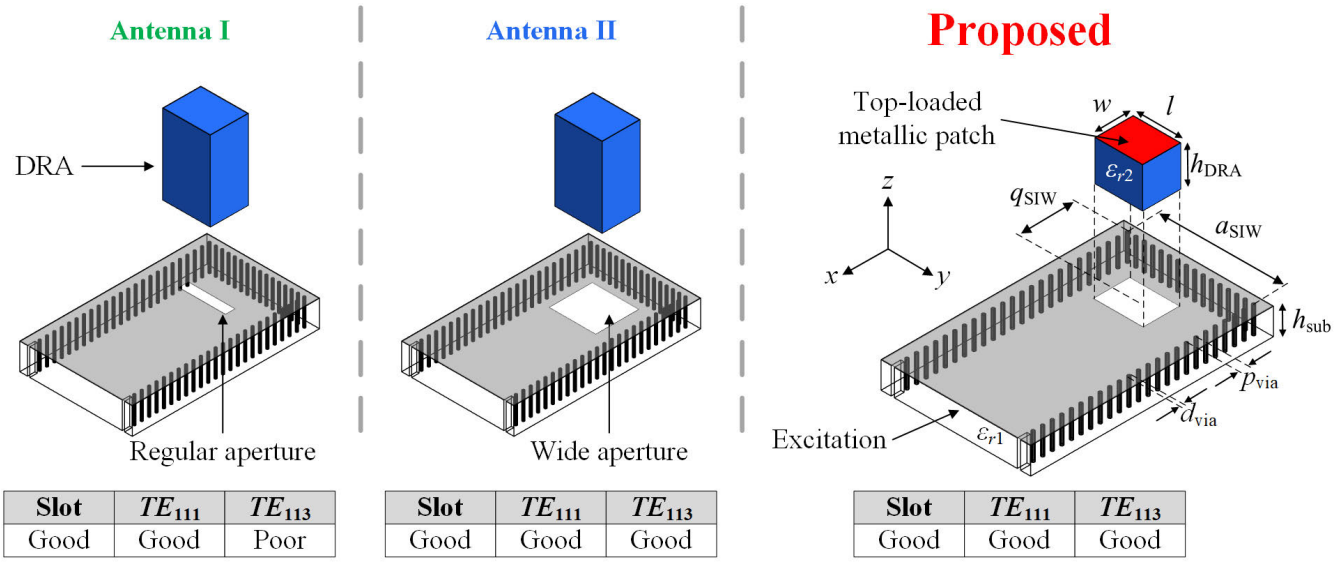

Slot	TE_{111}	TE_{113}
Good	Good	Poor

Slot	TE_{111}	TE_{113}
Good	Good	Good

Slot	TE_{111}	TE_{113}
Good	Good	Good

FIGURE 1. Evolution and configuration of the proposed antenna element.

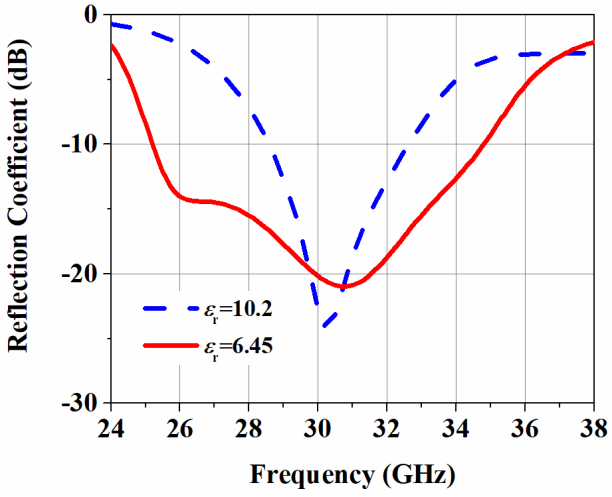

FIGURE 2. Simulated reflection coefficient of Antenna I under the permittivity of 10.2 and 6.45.

TABLE 1. Comparison of different antennas.

	Impedance Bandwidth (%)	DRA Volume (mm^3) ($L \times W \times H$)
Antenna I	32	2.9 × 2.3 × 3.4
Antenna II	40	2.9 × 1.8 × 3.6
Proposed	40	2.4 × 1.8 × 1.9

TABLE 2. Dimensions of the antenna element (unit: mm).

	SIW		Wide aperture	DRA	Top-loaded patch
Parameters	a_{SIW}	p_{via}	l_{slot}	l_{DRA}	l_{patch}
Values	5.7	0.5	2.4		
Parameters	q_{SIW}	d_{via}	w_{slot}	w_{DRA}	w_{patch}
Values	2.9	0.3	1.8		
Parameters	h_{sub}			h_{DRA}	
Values	1.524			1.9	
Parameters	ε_{r1}			ε_{r2}	
Values	3.55			6.45	

limited bandwidths that also hinder the potential applications of DRAs in millimetre-wave and even terahertz systems. Although methods of stacked DRAs [24], [25] and wideband dense-dielectric patches [26] can improve the impedance bandwidth by up to 25% and demonstrate the implementation of the large planar array, the complexity of the array is higher which may cause a fabrication uncertainty in real mmW products.

In this work, a new design of a wideband DRA and its array are presented. A wide aperture is used to excite a DRA element and form an antenna array configuration. The proposed approach tackles the bandwidth limitation for a single rectangular DRA and provides a wideband feature with stable radiation performance over the entire operating bandwidth. To further increase the antenna's bandwidth, the higher-order mode of the DRA is utilized. Combining both slot and DRA modes, the impedance bandwidth of the antenna can reach 40%. Meanwhile, the height of the DRA is reduced by approximately half after adding the top-loaded patch. To show a gain enhancement, a 1-to-8 SIW full-corporate feeding network is used to excite a 16-element antenna array. The final prototype of the array can achieve an impedance bandwidth of 35.5% from 25.5 to 36.5 GHz for the reflection coefficient ≤ -10 dB. Throughout the whole operating bandwidth, it maintains a stable unidirectional radiation pattern with cross-polarization levels under -22 dB, which is attractive for mmW applications.

This paper is organized as follows. The working principle, antenna configuration, performance and parametric studies

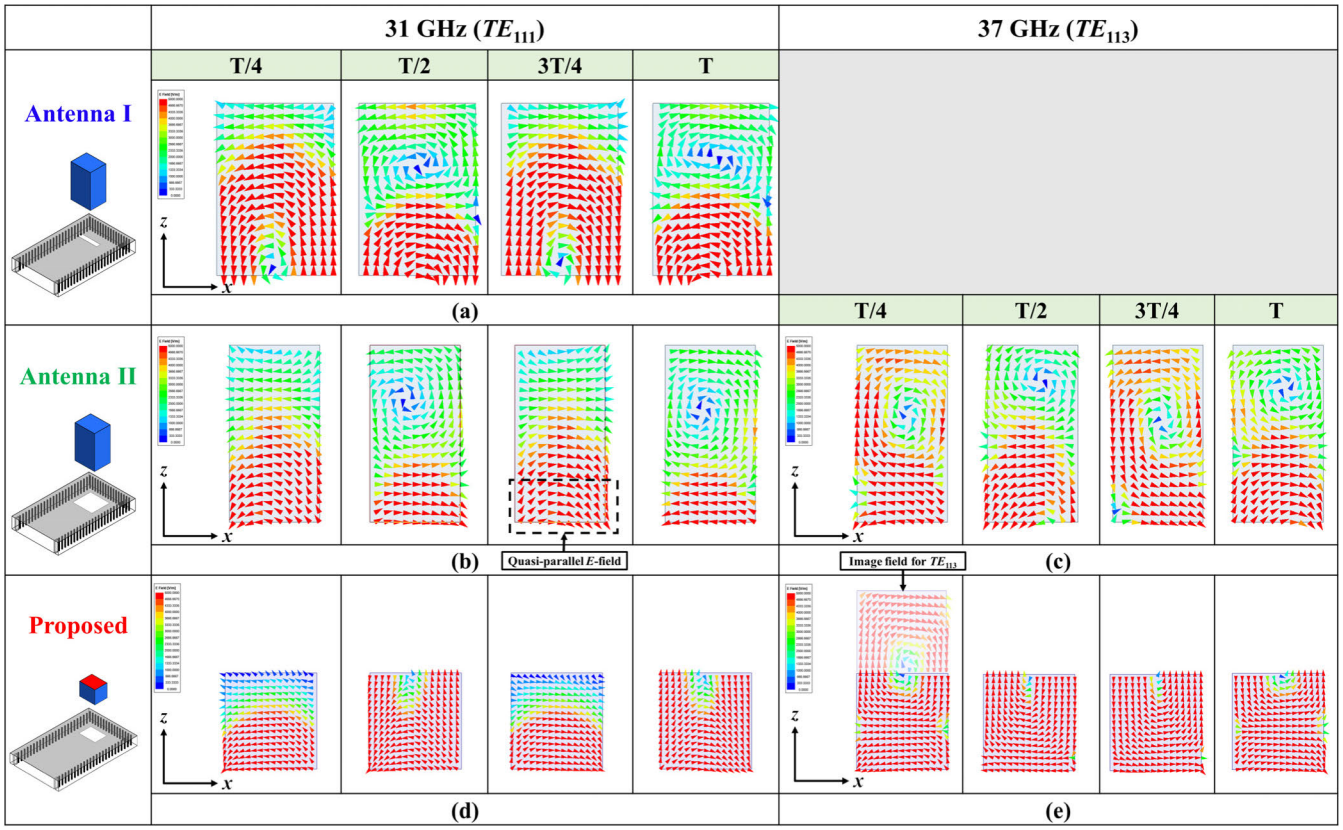

FIGURE 3. Simulated electric field (*E*-field) distributions inside the DRA of (a) Antenna I @ 31 GHz, (b) Antenna II @ 31 GHz, (c) Antenna II @ 37 GHz, (d) Proposed @ 31 GHz, and (e) Proposed @ 37 GHz.

of the proposed antenna element are discussed in Section II. The configuration and fabrication of the proposed antenna array are described in Section III, followed by Section IV which deals with the measurement, discussion of the proposed antenna array and comparison between other reported arrays. Finally, Section V presents the conclusion.

II. ANTENNA ELEMENT DESIGN

A. WORKING PRINCIPLE

The evolution of the proposed antenna element is shown in Fig. 1. Detailed values of the impedance bandwidth and DRA volume of each antenna are listed in Table 1. To begin with this, we designed a regular aperture-coupled DRA on a substrate-integrated waveguide (SIW) (denoted as Antenna I). Antenna I has two resonances that are well-matched at 26 and 31 GHz, which are contributed by the slot mode and the fundamental mode of the DRA (TE_{111}), respectively. Antenna I is similar to the antenna model in [17], where only TE_{111} is excited due to the higher permittivity of DRA. Fig. 2 shows the simulated reflection coefficient of Antenna I under the permittivity of 10.2 and 6.45. When the permittivity is 10.2, Antenna I only has a single resonance (TE_{111}) due to the high-quality factor (Q-factor) created by the high permittivity. This result shows Antenna I is able to generate both TE_{111} and the slot mode when the selection of the permittivity is near 6.45. Fig. 3 illustrates the simulated vector electric field (*E*-field) distributions inside the DRA of Antenna I (regular aperture-coupled DRA), Antenna II (wide aperture-coupled DRA) and Proposed (wide aperture-coupled DRA with top-loaded metallic patch) at 31 and 37 GHz, where all the distribution is along the *xoz*-plane and the scale of the field magnitude remains constant. Since the energy is coupled from the substrate to the DRA along the *z*-direction, the *E*-field distribution at time = T/4, T/2, 3T/4 and T shows that TE_{111} appeared in Antenna I at 31 GHz (Fig. 3(a)).

TABLE 3. Resonant frequency of DRA modes.

	TE_{111}	TE_{113}
Calculated frequency (GHz)	29.84	40.341
Simulated frequency (GHz)	31	37

To expand the bandwidth, we can incorporate the fundamental and higher-order modes of the DRA by increasing the size of the DRA [27]. However, this may lead to a large projection area of the element, which requires larger element spacing in the array configuration and thus limits the radiation performance. Instead of enlarging the radiator, we found that widening the excitation aperture under the DRA (denoted as Antenna II) can also incorporate both fundamental and higher-order modes together. The *E*-field distribution at time = T/4, T/2, 3T/4 and T shows that both TE_{111} and the higher-order mode of the DRA (TE_{113})

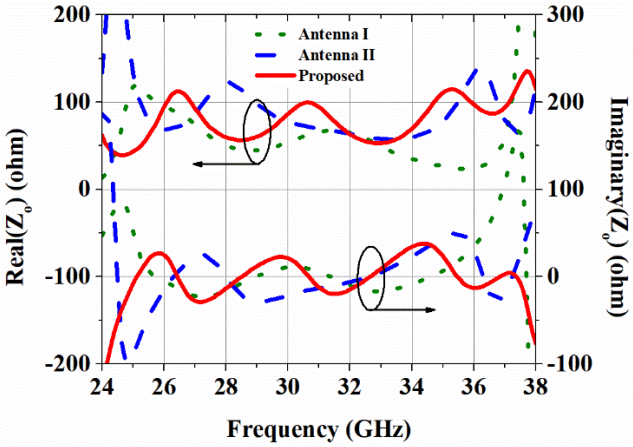

FIGURE 4. Simulated input impedance of Antenna I, Antenna II and proposed.

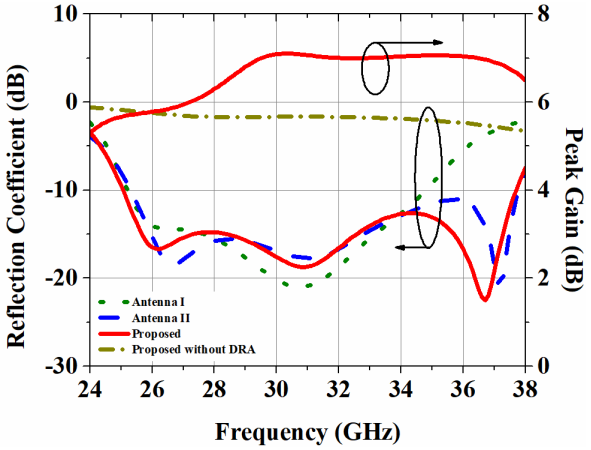

FIGURE 5. Simulated reflection coefficient of Antenna I, Antenna II and Proposed (w and w/o DRA) with the peak gain of proposed.

appeared in Antenna II (Fig. 3(b) and (c)). The use of a wide aperture to excite the DRA is effective in lowering the reactance of the higher-order mode (TE_{113}), which can be well-matched at high frequencies and incorporates with TE_{111} in the DRA. Due to the use of a wide aperture to excite the DRA, the radiation effect from the aperture would also contribute to the mode generation of the DRA. This influence can be observed in the field distributions at the time of T/2 and T of the mode TE_{111} at 31 GHz. Therefore, a null field is shown in the upper region of the DRA. After widening the excitation aperture, TE_{111} at 31 GHz is still being maintained as the condition of the regular aperture case, while TE_{113} is successfully excited at 37 GHz. It is worth mentioning that the E-field vectors in the area occupied by the aperture are quasi-parallel to the surface of the aperture due to the influence of the wide aperture radiation mode. To verify the existence of the DRA modes, the dielectric waveguide model (DWM) [28] is used to find out the resonant frequencies of TE_{111} and TE_{113}. Although the operating principle of this work may slightly differ from [28] since the feeding aperture and the dielectric constant of the substrate in [28] are different

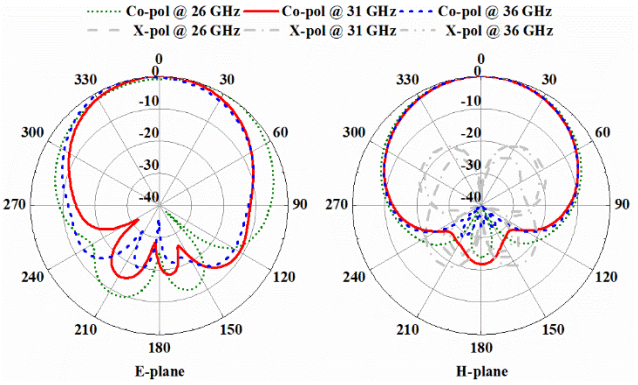

FIGURE 6. Simulated radiation patterns of the proposed antenna element.

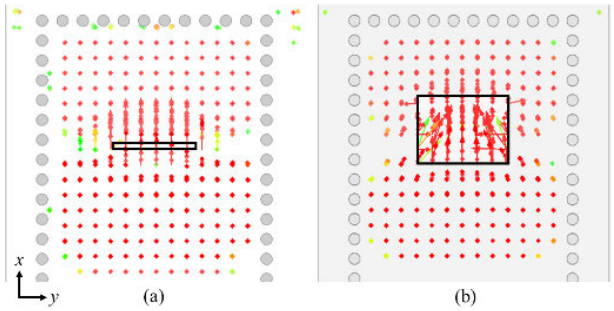

FIGURE 7. Simulated E-field distributions within (a) regular and (b) wide aperture.

from our proposed antenna, the equations listed in [28] are a good reference for designing the DRA. The characteristics equations of the wavenumbers k_x, k_y and k_z for the TE_{pqr} are listed as follows:

$$k_x a = p\pi - 2\tan^{-1}\left[k_x/(\varepsilon_r k_{x0})\right], p = 1, 2, 3\ldots$$
$$k_{x0} = \left[(\varepsilon_r - 1)\,k_0^2 - k_x^2\right]^{1/2} \quad (1)$$
$$k_y b = q\pi - 2\tan^{-1}\left[k_x/(\mu_r k_{y0})\right],$$
$$\mu_r = 1, q = 1, 2, 3\ldots$$
$$k_{y0} = \left[(\varepsilon_r - 1)\,k_0^2 - k_y^2\right]^{1/2} \quad (2)$$
$$2k_z d = r\pi - 2\tan^{-1}\left[k_x/(\varepsilon_r k_{z0})\right], r = 1, 2, 3\ldots$$
$$k_{z0} = \left[(\varepsilon_r - 1)\,k_0^2 - k_z^2\right]^{1/2} \quad (3)$$
$$k_x^2 + k_y^2 + k_z^2 = \varepsilon_r k_0^2 \quad (4)$$

where k_{x0}, k_{y0} and k_{z0} are decay constants of the field outside the DRA and k_0 is the free space wavenumber.

We applied the parameter of Antenna II: a=1.8mm, b=2.9mm, d=3.6mm and ε_r =6.45. By solving (1) – (4), the resonant frequency is calculated and compared with the simulated frequency in Table 3. The simulated results are matched to the calculated frequency which verifies that TE_{111} and TE_{113} modes are excited in the proposed design, and they correspond to the second and third resonance, respectively.

To reduce the profile of the antenna, a metallic patch is placed at the null of the electric field of TE_{111} and TE_{113}

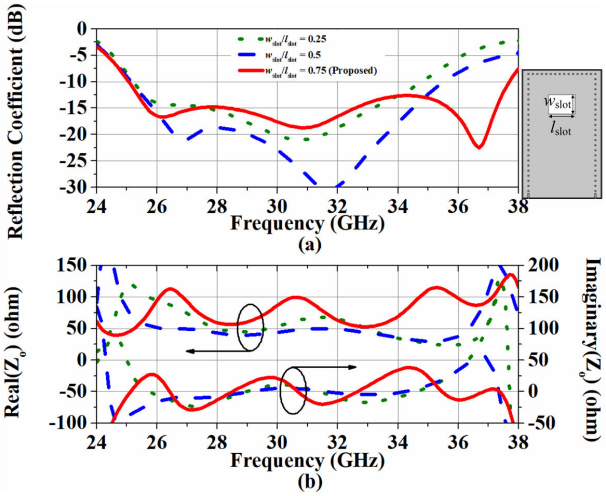

FIGURE 8. Simulated (a) reflection coefficient and (b) input impedance of the proposed antenna element under different ratios of the aperture.

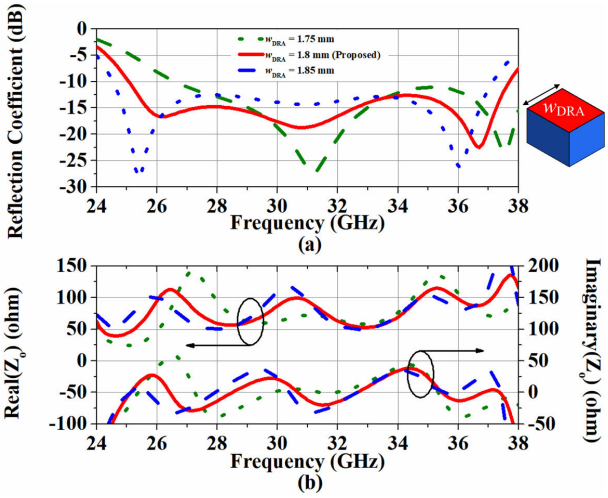

FIGURE 9. Simulated (a) reflection coefficient and (b) input impedance of the proposed antenna element under different values of DRA width.

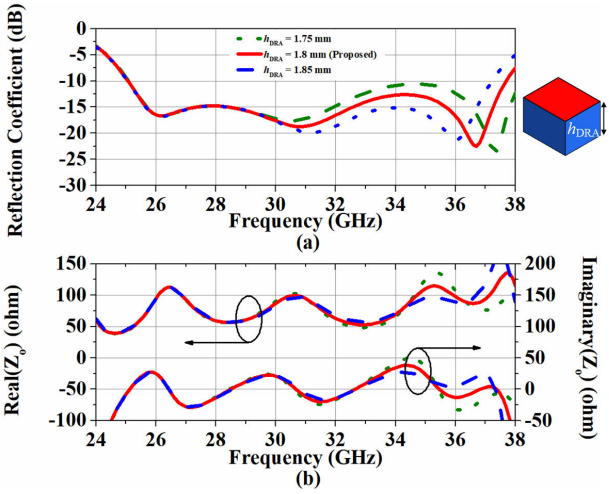

FIGURE 10. Simulated (a) reflection coefficient and (b) input impedance of the proposed antenna element under different values of DRA thickness.

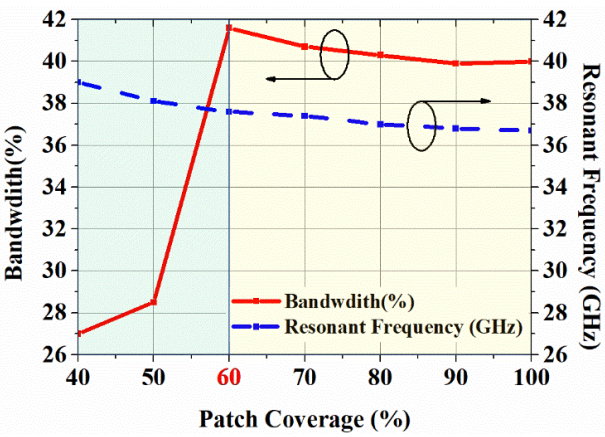

FIGURE 11. Bandwidth and resonant frequency of the third resonance under different areas of patch coverage.

modes (denoted as Proposed). This metallic patch forms the virtual ground for the DRA modes, so that the height of the DRA can be decreased from 3.6 to 1.9 mm. The E-field distribution at time = T/4, T/2, 3T/4 and T shows that TE_{111} and TE_{113} are consistent in the proposed element, as shown in Fig. 3(d) and (e), respectively.

Fig. 4 shows the simulated input impedance of Antenna I, Antenna II and Proposed. Antenna I (green dotted line) have a very high reactance at higher-order modes where the antenna is difficult to have good matching in its frequency response. After widening the aperture (blue dashed line), the reactance is lowered and converges around zero, which leads to a good impedance matching at the higher-order mode (TE_{113}). Therefore, the proposed design can have three resonances (slot, TE_{111} and TE_{113}) with good impedance matching and thus produces a wide impedance bandwidth of 40% from 25 to 38 GHz.

B. ANTENNA CONFIGURATION AND PERFORMANCE

In Fig. 1, it shows the configuration of the proposed antenna element. Detailed dimensions of the proposed element are listed in Table 2. In this design, a *Rogers RO4003C* (ε_r = 3.55 and tan σ = 0.0027) is used for the SIW section while a *Rogers RT/duroid 6006* (ε_r = 6.45 and tan σ = 0.0027) is used for the DRA. The SIW network is formed by three periodic rows of metallic vias, where TE_{01} mode is propagating for transmission. The period between the vias is 0.5 mm and the diameter of the via is 0.3 mm. The lower metallic surface of the SIW serves as a ground plane for the antenna. On the top metallic surface of the SIW, a wide aperture with length l_{slot} and width w_{slot} is etched 2.9mm away from the end of the SIW network for coupling the energy from the substrate to the DRA. This aperture is right under the DRA and has the same size as its base area ($l_{DRA} \times w_{DRA}$), where l_{DRA} and w_{DRA} are the length and width of the DRA, respectively. On the top surface of the DRA, a metallic patch with length l_{patch} and width w_{patch} is printed. For ease of fabrication, the

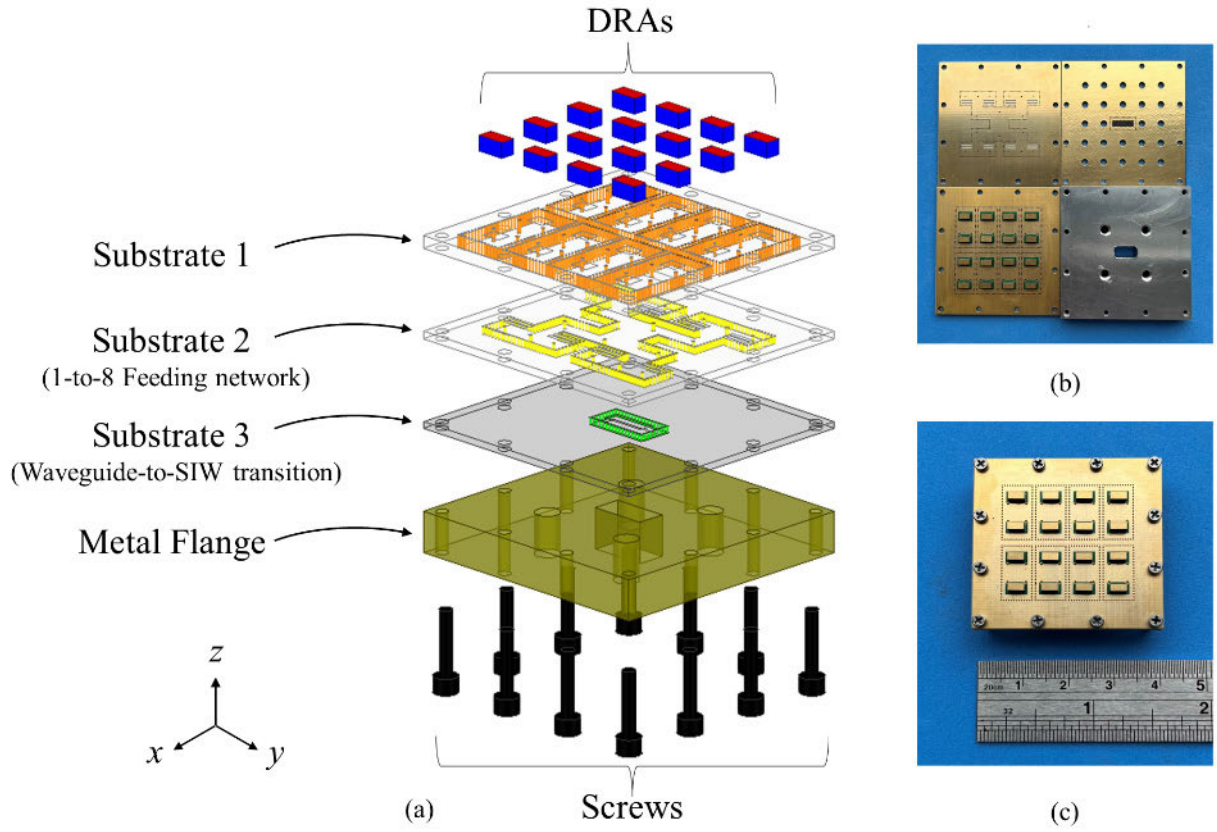

FIGURE 12. (a) Geometry of the proposed antenna array. (b) Photograph of different layers of the prototype. (c) Photograph of the prototype after assembly.

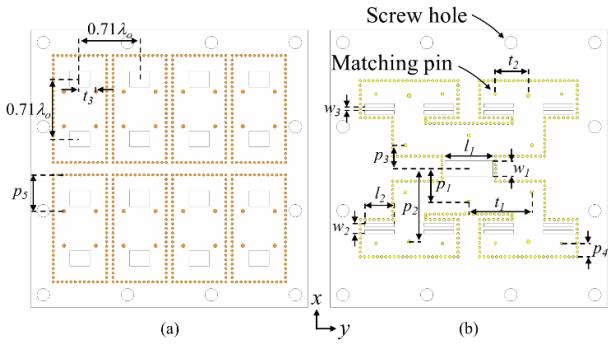

FIGURE 13. Feeding network of the proposed antenna array. Top view of (a) Substrate 1 and (b) Substrate 2.

TABLE 4. Dimensions of the antenna array (unit: mm).

Parameters	l_1	l_2	w_1	w_2	w_3
Values	6.74	3.56	1.88	1.27	0.32
Parameters	p_1	p_2	p_3	p_4	p_5
Values	3.93	8.69	1.31	1.58	4.3
Parameters	w_{slot}	w_{DRA}	l_{slot}	l_{DRA}	d_{via}
Values	1.86	1.86	2.37	3.6	0.3
Parameters	t_1	t_2	t_3	a_{SIW}	q_{SIW}
Values	7.53	3.95	1.9	6.35	2.81

size of the metallic patch is chosen to be equivalent to the base area of the DRA. As a result, the size of the aperture and patch together with the base area of the DRA are all identical, which are chosen as $w_{slot} = w_{DRA} = w_{patch} =$ 1.8 mm and $l_{slot} = l_{DRA} = l_{patch} = 2.4$ mm. The prototype was simulated by a commercial EM software Ansoft HFSS. Fig. 5 shows the simulated reflection coefficient and peak gain of the proposed antenna element in red solid lines. The impedance bandwidth of the proposed element is 40% covering from 25.1 to 37.7 GHz for the reflection coefficient $\leq$ -10 dB. Its peak gain value varies from 5.3 to 7.1 dBi. It is worth noting that if the DRA is absent from the proposed design, the slot mode cannot be matched and exhibits zero bandwidth. This implies that the DRA not only generates TE_{111} and TE_{113} but also provides a good matching for the slot mode. Fig. 6 introduces the simulated radiation patterns at 26, 31 and 36 GHz. Stable broadside radiation patterns can be observed throughout the whole operating bandwidth. The cross-polarization in the E-plane radiation patterns is under -40 dB which is not displayed.

It is worth mentioning that the wide aperture structure in this design is effective in widening the impedance bandwidth of the DRA by lowering the reactance at higher-order modes but causes a relatively large cross-polarization level

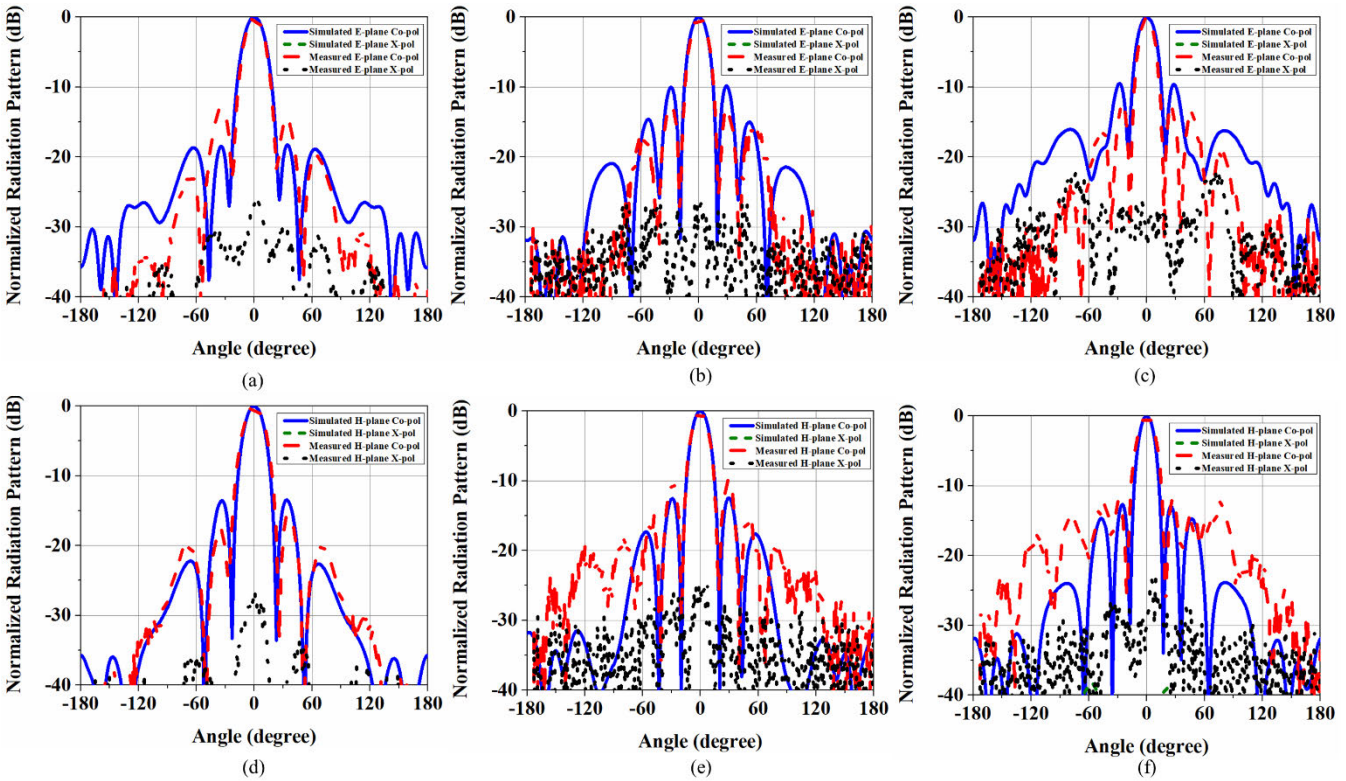

FIGURE 14. Simulated and measured radiation patterns of the proposed antenna array. (a) E-plane @ 27 GHz, (b) E-plane @ 31 GHz, (c) E-plane @ 35 GHz, (d) H-plane @ 27 GHz, (e) H-plane @ 31 GHz and (f) H-plane @ 35 GHz.

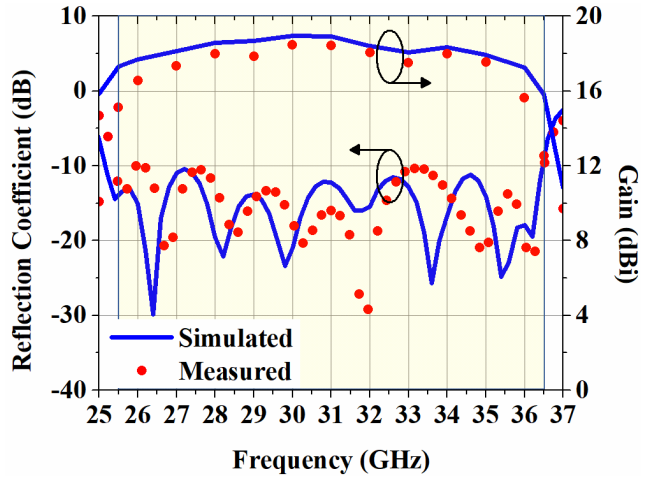

FIGURE 15. Measured and simulated results of both reflection coefficient and gain of the proposed antenna array.

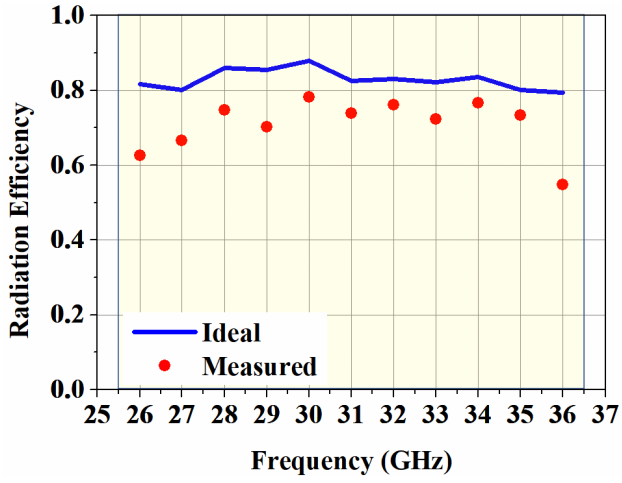

FIGURE 16. Ideal and measured radiation efficiency of the proposed antenna array.

of approximately -20 dB in the H-plane radiation patterns, while the cross-polarization in the E-plane radiation patterns is under −40 dB. Fig. 7 shows the comparison of the simulated E-field distributions for both regular and wide aperture cases. The E-field vectors within the regular aperture are distributed along the x-axis constantly; while a small amount of the E-field vectors in the wide aperture case are not purely distributed toward the x-axis, which causes a lower purity of polarization in the H-plane and results in −20 dB cross-polarization level.

C. PARAMETRIC STUDIES

To better understand the operating principle of the proposed antenna, we carried out a set of parametric studies. We examined the effect of different ratios of the aperture ($w_{\text{slot}}/l_{\text{slot}}$), DRA widths ($w_{\text{DRA}}$), DRA thicknesses ($h_{\text{DRA}}$)

TABLE 5. Comparison between the proposed unit and other reported rectangular DRA arrays.

Reference	Type of Elements	Feeding Technique	No. of elements	Centre frequency f_c (GHz)	Operating Bandwidth (%)		Peak Gain (dBi)	Front-to-back ratio at f_c (dB)	Element's projection area $L \times W$ (λ_0^2)
					Impedance	3-dB Gain			
[17]	SIW-fed DRA Array	SIW	4 × 1	37.8	4.7	15	11.7	9	0.38 × 0.19
[18]	SIW Hybrid feeding DRA Array	SIW	8 × 8	36	1.7	\	21.6	\	0.36 × 0.18
[20]	Template-Based DRA Array	Microstrip Line	2 × 2	60	12	13.5	10.5	\	1.27 × 1.27
[23]	SIW-integrated Parasitic DRA Array	SIW	1 × 4	37.2	8.9	9.4	12	\	0.37 × 0.19
[25]	Stacked SIW-fed DRA Array	SIW	4 × 4	67	16.4	18	17.2	\	0.40 × 0.40
[15]	Connected ring DRA Array	Microstrip Line	1 × 4	26.7	31.6	31.6	9.8	6	0.42 × 0.29
[16]	Connected ring DRA Array	Microstrip Line	1 × 4	27.3	29.6	29.6	10.7	10	0.47 × 0.30
[31]	Dielectric-loaded cavity-backed slot antenna	Microstrip Line	1 × 4	32.4	47.1	21.4	11.4	9.5	0.58 × 0.48
This work	Wide aperture-fed DRA (Fig. 1)	SIW	Single	31.4	40	40	7.1	21	0.25 × 0.19
	Wide aperture-fed DRA Array (Fig. 13)	SIW	4 × 4	31	35.5	32	18.5	31	0.37 × 0.19

and patch coverage in terms of reflection coefficient and input impedance. These parameters are found to have a more significant effect on impedance matching. During the parametric study of w_{DRA}, h_{DRA} and the size of the patch, only one of the parameters is varied while the rest of it remains unchanged.

Firstly, the effect of $w_{\mathrm{slot}}/l_{\mathrm{slot}}$ on the reflection coefficient and input impedance is shown in Fig. 8. When the ratio equals 0.25 (regular aperture), the reactance in high frequencies is large and over 100 Ω, so that the antenna cannot be matched. When the ratio equals 0.5, the reactance is lowered to 50 Ω. When the ratio changes from 0.25 to 0.75 (proposed wide aperture), the reactance curve converges around zero. This obtained result confirms that the wide aperture is effective in lowering the reactance at high frequencies (TE_{113}) at 37 GHz and thus expands the bandwidth together with the slot mode and the TE_{111} of the DRA.

Secondly, the effect of w_{DRA} on the reflection coefficient and input impedance is shown in Fig. 9. When w_{DRA} is increased, both first and third resonances are shifted to lower frequencies and vice versa. w_{DRA} only affects the impedance matching of the second resonance but not its resonant frequency. This is because the wide aperture is also a factor contributing to the DRA modes in the proposed design. As mentioned before, the DRA not only generates TE_{111} and TE_{113} but also provides a good matching for the slot mode. Therefore, the DRA width should be optimized to maintain all three resonances having good matching to contribute to the wide bandwidth. The optimal case is chosen as $w_{\mathrm{DRA}} = 1.8$ mm.

Thirdly, the effect of h_{DRA} on the reflection coefficient and input impedance is shown in Fig. 10. When h_{DRA} is varied, only the third resonance is greatly influenced. This is because the third resonance is contributed by TE_{113}, where the higher-order mode is generated along the z-direction (along the height of the DRA). Therefore, the third resonance is sensitive to the DRA thickness. When h_{DRA} is decreased, the third resonance is shifted to the higher frequencies, which shows the potential for wider bandwidth. However, 1.85 mm is a non-standard thickness of the laminate used for the DRA, which may increase the uncertainty in fabrication. Therefore, the optimal case is to choose the standard thickness of that laminate, which is $h_{\mathrm{DRA}} = 1.9$ mm.

Fourthly, Fig. 11 illustrates the impedance bandwidth and the resonant frequency of the third resonance under different areas of patch coverage. During the parametric studies, we only varied the size of the patch to achieve different coverage on the DRA. The resonant frequency of the third resonance is slightly affected by varying the size of the patch because this mode is contributed by TE_{113}. Moreover, the impedance bandwidth started to have a dramatic increase when the coverage approached 60%, which is electrically large enough to act as a virtual ground for the DRA modes. Although the impedance bandwidth is the highest, 42% when the coverage is 60%, further increasing the size of the patch only caused a slight bandwidth deduction from 42% to 40%.

For ease of fabrication, we finally chose the size of the patch to be equivalent to the base area of the DRA.

III. ANTENNA ARRAY DESIGN

To improve the gain performance, a 16-element DRA array is designed based on the proposed antenna element, which is shown in Fig. 12(a). The proposed array is built on two *Rogers 4003C*Substrates 1 and 2, one of which has a thickness of 1.575 mm while the other one is 0.912 mm. It should be mentioned that the thickness of 0.912 mm is a combination of two Rogers 4003 with 0.406 mm and one bonding film *Rogers 4350B* ($\varepsilon_r = 3.66$) with 0.1 mm in between. A *Rogers RT/duroid 5880* ($\varepsilon_r = 2.2$ and $\tan\sigma = 0.009$) with a thickness of 0.787 mm is placed under Substrate 1 and 2 for designing the SIW-to-waveguide transition. On the other hand, an aluminium waveguide flange is located at the bottom for measurement. All the substrates and the aluminium board are aligned and fixed by 12 metallic screws. Additionally, there are green markings on Substrate 1 (Fig. 12(c)) to indicate the position of each DRA, where a good alignment can be confirmed. With the help of glue and a tweezer, the DRA is attached at the centre of each coupling aperture on Substrate 1. To ensure reliable measurement data, multiple prototypes are implemented using the stated method and then measured.

A 1-to-8 full-corporate feeding network with equal phase and amplitude [29] is designed to excite 16 elements, which is shown in Fig. 13. Detailed dimensions of the antenna array are listed in Table 4. The spacing between each antenna element is 0.71 λ_o in both x- and y- directions, where λ_o is the wavelength in free space at the centre frequency. With such a spacing, the proposed array is found to achieve the maximum gain. The feeding network is symmetrical in both x- and y-directions while the waveguide-to-SIW transition is built at the centre. This arrangement helps contribute to a stable unidirectional radiation pattern with low cross-polarization levels throughout the operating bandwidth. In addition, a thin copper strip is placed at the centre of the coupling aperture on the top layer of Substrate 2. This arrangement helps produce a good impedance matching over a wide frequency range for the SIW-to-waveguide transition [30].

Mutual coupling is a common phenomenon in antenna arrays, which is found disadvantageous to the radiation performance such as narrower bandwidth. In our design, we keep the mutual coupling and further optimize the antenna array. As a result, the elements are modified to be slightly larger than the wide aperture under them in the y-direction. This is different from the configuration mentioned in Section II-B.

IV. MEASUREMENT RESULTS AND DISCUSSION

Prototypes of the antenna array were fabricated and measured for verification. Fig. 12 shows the photographs of the fabricated prototypes. The measurement is calibrated and measured with a WR-28 waveguide module. The array and the waveguide flange are fixed by metallic screws. The total size is $40 \times 40 \times 9.2$ mm^3. During the measurement, the metallic screws ensure good electrical contact between each layer. Therefore, conductive adhesive film is not required in our design.

A. EXPERIMENTAL RESULTS

The reflection coefficient was measured by *Agilent E8361A* vector network and the radiation performance was performed in a compact range test system. The gain performance was calculated by comparing the measured results with the data of a standard gain horn. The simulated results were optimized and obtained through *Ansoft HFSS* software.

The simulated and measured radiation patterns in both E- and H-planes at 27, 31 and 35 GHz are displayed in Fig. 14. The measured main lobes remain stable over the measured bandwidth and agree well with the simulation. The measured half-power beamwidth in the E-plane varies from 19.5° to 21.5° while that in the H-plane varies from 15.3° to 20.1°. The simulated sidelobe levels are relatively large, which is caused by the large element spacing together with the mutual coupling inside the array. The measured sidelobe levels in the E-plane throughout the whole operating bandwidth are around −13 dB on average. The measured sidelobe levels in the H-plane are below −10 dB. The measured sidelobe levels show a discrepancy with the simulation and it becomes the most obvious at 27 GHz. The fabrication error of the prototypes may cause this. The measured cross-polarization levels are below −22 dB in the E-plane and below −23 dB in the H-plane. The simulated cross-polarization levels are not displayed because it is smaller than −40 dB over the entire operating bandwidth in both E- and H-planes. This is worth mentioning that the resultant magnetic field (H-field) vectors inside the 2×1 sub-array in Substrate 1 are purely pointing towards the y-direction, which suppresses the cross-polarization levels.

Fig. 15 shows the proposed antenna array's reflection coefficient and gain performance in both simulated and measured results, where the shaded area is the measured operating bandwidth. The results show a good agreement between the simulation and the measurement. The measured result shows that the prototype achieved an impedance bandwidth of 35.5% covering from 25.5 to 36.5 GHz for the reflection coefficient ≤ -10 dB. The maximum gain is 18.5 dBi at 30 GHz and the measured 3-dB gain bandwidth is 32% from 25.7 to 35.6 GHz. The ideal and measured radiation efficiency is plotted in Fig, 16, where the shaded area is the measured operating bandwidth. The maximum measured radiation efficiency is 78% at 30 GHz. The glues for attaching the antenna elements, fabrication errors, loss in the cable, and the loss in the adapter connected with the waveguide excitation port may cause discrepancies between the measured and simulated results.

B. COMPARISON AND DISCUSSION

A comparison of performance between the proposed antenna array and other reported rectangular DRA arrays in the mmW band is summarized in Table 5. For the DRA arrays reported in [17] and [18], they only operate at the fundamental

mode, which produces less than 10% impedance bandwidth. To expand the bandwidth, extra resonances can be introduced by adding parasitic elements [23] and using a stacked structure [20], [25], where the DRA arrays can produce up to 16.4% bandwidth, but the results are still far away from the performance of DRA reviewed in the microwave band. Recently, connected ring DRA arrays have been proposed in [15] and [16], which can produce over 30% in both impedance and 3-dB bandwidths. However, the microstrip line feeding method creates large back lobe radiation, which reduces the front-to-back ratio (FTBR). To maximize the bandwidth, cavity mode and slot mode are combined with the DRA mode to contribute a wide bandwidth of 47.1% [31], which creates the widest bandwidth among all the reported DRA arrays. However, it has a relatively narrower 3-dB gain bandwidth (21.4%). Same as [15] and [16], the DRA in [31] is fed by the microstrip line, which causes a low FTBR. It is worth mentioning that the proposed array uses a similar approach as [31] but with a simple design and a different excitation method and thus produces different radiation characteristics. In addition, [15], [16], and [31] all have a long length in their DRA element, which requires a large element spacing along that direction and thus limits the array radiation performance. Therefore, the aforementioned designs are only implemented into a linear array instead of a planar array. Compared with the reported arrays, the proposed array has a wide impedance bandwidth (35.5%) due to the use of a wide aperture to excite the DRA elements of the array. From the parametric study of this work, we confirm that the wide aperture acts as a resonator as well as excites TE_{111} and TE_{113} of the DRA. The slot mode and the two DRA modes are combined to contribute stable and directive radiation patterns to the broadside direction; therefore, a wide gain bandwidth (32%) can also be obtained which is the widest among the reported designs. Simultaneously, the SIW feeding network confirms a well FTBR in the proposed array (31 dB), which is the largest among the reported designs.

The fifth generation (5G) new radio (NR) is the latest standard for air interface in mobile communication networks, which is divided into frequency ranges 1 (FR1) and 2 (FR2). FR1 is referred to as 0.410 – 7.125 GHz while FR2 is referred to as 24.250 – 71.000 GHz. Within the FR2, the band n257 (26.5 – 29.5 GHz) is identified for local multipoint distribution service (LMDS) and band n261 (27.5 – 28.35 GHz) is identified to serve the applications in Ka-band (26.5 – 40 GHz). The proposed antenna covers the frequency range from 25 to 38 GHz, which is favourable to be used for wireless communications in the 5G NR bands n257/n261.

V. CONCLUSION

In this paper, we introduce a new design of a wide aperture-fed DRA and its array that can achieve wideband performance in the mmW band. The usage of a wide aperture achieves wideband performance which fully utilizes the potential of DRA. The top-loading patch acts as a virtual ground for the DRA modes and thus reduces the antenna profile. Using the full-corporate feeding network helps maintain stable radiation patterns with low cross-polarization levels over a wide frequency range. The proposed array obtained an impedance bandwidth of 35.5% from 25.5 to 36.5 GHz (for the reflection coefficient $\leq$ -10 dB) and a maximum gain of 18.5 dBi. By comparing with the reported reference, the proposed array has the widest 3-dB gain bandwidth and the largest front-to-back ratio. The proposed antenna and its array are good candidates for recent and future millimetre-wave wireless communication systems in the 5G NR bands n257/n261.

REFERENCES

[1] W. Hong, Z. H. Jiang, C. Yu, J. Zhou, P. Chen, Z. Yu, H. Zhang, B. Yang, X. Pang, M. Jiang, Y. Cheng, M. K. T. Al-Nuaimi, Y. Zhang, J. Chen, and S. He, "Multibeam antenna technologies for 5G wireless communications," *IEEE Trans. Antennas Propag.*, vol. 65, no. 12, pp. 6231–6249, Dec. 2017.

[2] J. G. Andrews, S. Buzzi, W. Choi, S. V. Hanly, A. Lozano, A. C. K. Soong, and J. C. Zhang, "What will 5G be?" *IEEE J. Sel. Areas Commun.*, vol. 32, no. 6, pp. 1065–1082, Jun. 2014.

[3] S. Long, M. McAllister, and L. Shen, "The resonant cylindrical dielectric cavity antenna," *IEEE Trans. Antennas Propag.*, vol. AP-31, no. 3, pp. 406–412, May 1983.

[4] K. M. Luk and K. W. Leung, *Dielectric Resonator Antennas*. Baldock, U.K.: Research Studies, 2003.

[5] H. Y. Lo, K. W. Leung, K. M. Luk, and E. K. N. Yung, "Low profile triangular dielectric resonator antenna," in *IEEE Antennas Propag. Int. Symp. Dig.*, vol. 4, Jul. 2000, pp. 2088–2091.

[6] S.-M. Deng, T.-W. Chen, and H.-H. Kan, "A CPW-fed rectangular dielectric resonator antenna," in *Proc. APMC Asia–Pacific Microw. Conf.*, 2001, pp. 954–957.

[7] X. L. Liang and T. A. Denidni, "H-shaped dielectric resonator antenna for wideband applications," *IEEE Antennas Wireless Propag. Lett.*, vol. 7, pp. 163–166, 2008.

[8] T.-H. Chang, Y.-C. Huang, W.-F. Su, and J.-F. Kiang, "Wideband dielectric resonator antenna with a tunnel," *IEEE Antennas Wireless Propag. Lett.*, vol. 7, pp. 275–278, 2008.

[9] A. Ittipiboon, A. Petosa, D. Roscoe, and M. Cuhaci, "An investigation of a novel broadband dielectric resonator antenna," in *IEEE Antennas Propag. Soc. Int. Symp. Dig.*, Jul. 1996, pp. 2038–2041.

[10] K. W. Leung, K. M. Luk, K. Y. Chow, and E. K. N. Yung, "Bandwidth enhancement of dielectric resonator antenna by loading a low-profile dielectric disk of very high permittivity," *Electron. Lett.*, vol. 33, no. 9, pp. 725–726, 1997.

[11] A. A. Kishk, X. Zhang, A. W. Glisson, and D. Kajfez, "Numerical analysis of stacked dielectric resonator antennas excited by a coaxial probe for wideband applications," *IEEE Trans. Antennas Propag.*, vol. 51, no. 8, pp. 1996–2006, Aug. 2003.

[12] A. G. Walsh, C. S. DeYoung, and S. A. Long, "An investigation of stacked and embedded cylindrical dielectric resonator antennas," *IEEE Antennas Wireless Propag. Lett.*, vol. 5, pp. 130–133, 2006.

[13] M.-D. Yang, Y.-M. Pan, Y.-X. Sun, and K.-W. Leung, "Wideband circularly polarized substrate-integrated embedded dielectric resonator antenna for millimeter-wave applications," *IEEE Trans. Antennas Propag.*, vol. 68, no. 2, pp. 1145–1150, Feb. 2020.

[14] M. M. M. Ali, M. Al-Hasan, I. B. Mabrouk, and T. A. Denidni, "Ultra-wideband hybrid magneto-electric dielectric-resonator dipole antenna fed by a printed RGW for millimeter-wave applications," *IEEE Access*, vol. 10, pp. 2028–2036, 2022.

[15] Y.-T. Liu, B. Ma, S. Huang, S. Wang, Z. J. Hou, and W. Wu, "Wideband low-profile connected rectangular ring dielectric resonator antenna array for millimeter-wave applications," *IEEE Trans. Antennas Propag.*, vol. 71, no. 1, pp. 999–1004, Jan. 2023.

[16] Y.-T. Liu, W. Zhao, B. Ma, S. Huang, J. Ren, W. Wu, H.-Q. Ma, and Z. J. Hou, "1-D wideband phased dielectric resonator antenna array with improved radiation performance using characteristic mode analysis," *IEEE Trans. Antennas Propag.*, vol. 71, no. 7, pp. 6179–6184, Jul. 2023.

[17] W. M. Abdel-Wahab, D. Busuioc, and S. Safavi-Naeini, "Millimeter-wave high radiation efficiency planar waveguide series-fed dielectric resonator antenna (DRA) array: Analysis, design, and measurements," *IEEE Trans. Antennas Propag.*, vol. 59, no. 8, pp. 2834–2843, Aug. 2011.

[18] W. M. Abdel-Wahab, Y. Wang, and S. Safavi-Naeini, "SIW hybrid feeding network-integrated 2-D DRA array: Simulations and experiments," *IEEE Antennas Wireless Propag. Lett.*, vol. 15, pp. 548–551, 2016.

[19] H. Chu and Y.-X. Guo, "A novel approach for millimeter-wave dielectric resonator antenna array designs by using the substrate integrated technology," *IEEE Trans. Antennas Propag.*, vol. 65, no. 2, pp. 909–914, Feb. 2017.

[20] A. A. Qureshi, D. M. Klymyshyn, M. Tayfeh, W. Mazhar, M. Börner, and J. Mohr, "Template-based dielectric resonator antenna arrays for millimeter-wave applications," *IEEE Trans. Antennas Propag.*, vol. 65, no. 9, pp. 4576–4584, Sep. 2017.

[21] M. S. Abdallah, Y. Wang, W. M. Abdel-Wahab, and S. Safavi-Naeini, "Design and optimization of SIW center-fed series rectangular dielectric resonator antenna array with 45° linear polarization," *IEEE Trans. Antennas Propag.*, vol. 66, no. 1, pp. 23–31, Jan. 2018.

[22] L. Lu, Y.-C. Jiao, Z.-B. Weng, L. Zhang, C.-Y. Cui, and R.-Q. Wang, "High-efficiency circularly polarized dielectric resonator antenna array fed by the cavity-backed SIW," *IEEE Antennas Wireless Propag. Lett.*, vol. 17, no. 7, pp. 1145–1148, Jul. 2018.

[23] W. M. Abdel-Wahab, M. Abdallah, J. Anderson, Y. Wang, H. Al-Saedi, and S. Safavi-Naeini, "SIW-integrated parasitic DRA array: Analysis, design, and measurement," *IEEE Antennas Wireless Propag. Lett.*, vol. 18, no. 1, pp. 69–73, Jan. 2019.

[24] W.-W. Yang, W.-J. Sun, H. Tang, and J.-X. Chen, "Design of a circularly polarized dielectric resonator antenna with wide bandwidth and low axial ratio values," *IEEE Trans. Antennas Propag.*, vol. 67, no. 3, pp. 1963–1968, Mar. 2019.

[25] Z. Chen, C. Shen, H. Liu, X. Ye, L. Qi, Y. Yao, J. Yu, and X. Chen, "Millimeter-wave rectangular dielectric resonator antenna array with enlarged DRA dimensions, wideband capability, and high-gain performance," *IEEE Trans. Antennas Propag.*, vol. 68, no. 4, pp. 3271–3276, Apr. 2020.

[26] Y. Li and K.-M. Luk, "Wideband perforated dense dielectric patch antenna array for millimeter-wave applications," *IEEE Trans. Antennas Propag.*, vol. 63, no. 8, pp. 3780–3786, Aug. 2015.

[27] L. Y. Feng and K. W. Leung, "Millimeter-wave wideband dielectric resonator antenna," in *Proc. 40th Int. Conf. Infr., Millim., Terahertz Waves (IRMMW-THz)*, Aug. 2015, pp. 1–2.

[28] Y.-M. Pan, K. W. Leung, and K.-M. Luk, "Design of the millimeter-wave rectangular dielectric resonator antenna using a higher-order mode," *IEEE Trans. Antennas Propag.*, vol. 59, no. 8, pp. 2780–2788, Aug. 2011.

[29] G.-H. Sun and H. Wong, "C-shaped open slot antenna array for millimeter-wave applications," *IEEE Trans. Antennas Propag.*, vol. 69, no. 12, pp. 8426–8435, Dec. 2021.

[30] G.-H. Sun and H. Wong, "A planar millimeter-wave antenna array with a pillbox-distributed network," *IEEE Trans. Antennas Propag.*, vol. 68, no. 5, pp. 3664–3672, May 2020.

[31] A. A. Omar, J. Park, W. Kwon, and W. Hong, "A compact wideband vertically polarized end-fire millimeter-wave antenna utilizing slot, dielectric, and cavity resonators," *IEEE Trans. Antennas Propag.*, vol. 69, no. 9, pp. 5234–5243, Sep. 2021.

KING TUNG LO (Student Member, IEEE) was born in Hong Kong. He received the B.Eng. degree in electrical engineering from the City University of Hong Kong, in 2021, where he is currently pursuing the Ph.D. degree. His current research interests include the DRA and wideband elements. He was a recipient of HKPFS in 2020.

HANG WONG (Fellow, IEEE) received the B.Eng., M.Phil., and Ph.D. degrees in electronic engineering from the City University of Hong Kong (CityU), in 1999, 2002, and 2006, respectively. He joined the Department of Electrical Engineering, CityU, in 2012. He had several visiting professorships with Stanford University, USA; University of Waterloo, Canada; University of College London, U.K.; and University of Limoges, France, in 2011, 2013, 2014, and 2015, respectively. He is currently the Director of the Applied Electromagnetics Laboratory, CityU, and the Deputy Director of the State Key Laboratory of Terahertz and Millimeter Waves, Hong Kong. He has over 250 publications, two coauthors of book chapters, and 30 U.S. and Chinese patents. His research interests include the antenna technologies of 5G, 6G, millimeter-wave, and terahertz applications. His achievements led to receiving numerous awards at local, national, and international conferences. For example, he received the Best Paper Award at the National Conference *2017 Les Journées Nationales Microondes*, France; the Best Paper Award at the 2017 IEEE International Workshop on Electromagnetics, U.K.; the Best Associate Editor Award 2016 of an IEEE ANTENNAS AND WIRELESS PROPAGATION LETTERS, USA; and the Outstanding Scientist Award of 2016 presented by Shenzhen Science and Technology Bureau, Shenzhen. He was awarded to lead a major project supported by the Ministry of Industry and Information Technology of PRC to develop new antenna elements for TD-LTE and 5G applications. He was the Chair of the IEEE Hong Kong Section of the Antennas and Propagation (AP)/Microwave Theory and Techniques (MTT) Chapter, from 2011 to 2004 and from 2022 to 2024. He was the IEEE APS Region-10 Representative 2015–2021. He was the General Co-Chair of the Asia–Pacific Microwave Conference (AMPC) 2020, Hong Kong; the General the Chair of the Cross-Strait Radio Science and Wireless Technology Conference 2021, Shenzhen, China; and the General Chair of the IEEE International Workshop on Electromagnetics 2025, Hong Kong. He is an Associate Editor of IEEE TRANSACTIONS ON ANTENNAS AND PROPAGATION and IEEE ANTENNAS AND WIRELESS PROPAGATION LETTERS.